Tensile Loading of Double-Walled and Triple-Walled Carbon Nanotubes and their Mechanical Properties

ARTICLE *in* THE JOURNAL OF PHYSICAL CHEMISTRY C · OCTOBER 2009

Impact Factor: 4.77 · DOI: 10.1021/jp902471q

5 AUTHORS, INCLUDING:

Xianlong Wei
Peking University
59 PUBLICATIONS **968** CITATIONS
SEE PROFILE

Qing Chen
Peking University
173 PUBLICATIONS **6,020** CITATIONS
SEE PROFILE

Lian-Mao Peng
Peking University
396 PUBLICATIONS **9,752** CITATIONS
SEE PROFILE

Rongli Cui
30 PUBLICATIONS **532** CITATIONS
SEE PROFILE

Tensile Loading of Double-Walled and Triple-Walled Carbon Nanotubes and their Mechanical Properties

Xianlong Wei,[†] Qing Chen,*[,†] Lian-Mao Peng,[†] Rongli Cui,[‡] and Yan Li[‡]

Key Laboratory for the Physics and Chemistry of Nanodevices and Department of Electronics, and College of Chemistry and Molecular Engineering, Peking University, Beijing 100871, People's Republic of China

Received: March 19, 2009; Revised Manuscript Received: August 10, 2009

The mechanical response of individual double-walled and triple-walled carbon nanotubes (CNTs) and CNT ropes consisting of only two double-walled CNTs under tensile load was measured using nanomanipulators in a scanning electron microscope. The breaking strain and strength and Young's modulus of individual CNTs were measured to be 1.5−4.9%, 13−46 GPa, and 0.73−1.33 TPa, respectively. The low breaking strain and strength are most likely caused by the defects presented in the measured CNTs synthesized by chemical vapor deposition. Carbon nanotube ropes exhibited one-step or stepwise breaks depending on the relative breaking strains of the two CNTs.

1. Introduction

The mechanical response of carbon nanotubes (CNTs) under tensile load has been the focus of many experimental and theoretical studies due to their high tensile strength and promising applications in many aspects, such as reinforcements in composites.[1] Tensile loading of individual multiwalled carbon nanotubes (MWCNTs) achieved first by Yu et al. exhibited a tensile strength of 63 GPa and a breaking strain of 12%.[2] The breaking strain of a single-walled carbon nanotube (SWCNT) was also reported to reach 12%.[3] However, several other experimental results indicated that both individual MWCNTs[4−6] and SWCNT ropes[7,8] break at a strain less than about 6%, which is much smaller than various theoretical values evaluated for defect-free SWCNTs. Molecular mechanics simulations based on empirical force fields predicted a fracture strain of 10−15% and a fracture stress of 65−93 GPa,[9] while quantum mechanics simulations predicted that fracture strain and tensile strength of a defect-free CNTs in the low-temperature limit could be 20−30% and over 100 GPa depending on the chirality.[10,11] By assuming that CNT failure is determined by activation and propagation of stress-induced Stone-Wales defects[12−15] and using a transition state theory, researchers have predicted that the fracture strain of a CNT under realistic temperatures and strain rates are diameter dependent.[14,15] A micrometer-long (20, 0) CNT under 300 K and stretched with a strain rate of 1%/h was predicted to yield at about 11 ± 1% based on molecular dynamics simulations with empirical potential.[14] On the basis of density functional theory, the fracture strain of a SWCNT in a room-temperature loading test with durations of 1 s was calculated to be about 18−22% depending on the chirality of the SWCNT.[15] Recently, Peng et al. reported the measurement of near-ultimate strength of MWCNTs of 110 GPa, and this is in excellent agreement with quantum mechanics predictions.[16]

Although the experimental values of the breaking strain or strength seem to agree with the theoretical results in some reports,[2,7,13,14,16] the experimentally measured CNTs were either individual thick MWCNTs consisting of many shells or SWCNT ropes consisting of many tubes, while the theoretical simulations were carried out mostly on individual thin SWCNTs. Moreover, breaking strain of CNTs has been predicted to increase with tube diameter,[12,14,15] and the interaction between tube shells in a MWCNT and tubes in a SWCNT rope may complicate the mechanical responses of the CNTs under tensile load. Therefore, for a quantitative comparison, it is desired to measure individual SWCNTs or CNTs with only a few shells that can be simulated by theoretical calculations. Nevertheless, the tensile loading of such thin-shelled small-diameter CNTs with strain and stress measured simultaneously has been rarely reported due to the difficulty in carrying out the experiments.

Here, with the method we recently developed for mechanical measurements on individual small-diameter CNTs using nanomanipulators in a scanning electron microscope (SEM), the breaking strain and strength and Young's modulus of individual double-walled CNTs (DWCNTs), triple-walled CNTs (TWCNTs), and CNT ropes consisting only two DWCNTs were measured by tensile loading. In the absence of experimental study of individual SWCNTs with strain and stress measured simultaneously, the presently measured individual DWCNTs and TWCNTs are the thinnest CNTs with the simplest intershell interaction among all the CNTs studied experimentally by now, which makes it possible to quantitatively compare with theoretical simulations. The presently measured CNT ropes consisting of only two CNTs provide the simplest cases for studying the breaking mechanism of CNT ropes.

2. Experimental Method

Our experiments were performed using Kleindiek MM3A nanomanipulators installed inside a FEI XL30F SEM. Thin-shelled CNTs grown across microtrenches on a SiO_2/Si substrate were used for the measurements. The CNT samples were synthesized at 960 °C with $FeCl_3$ as the catalytic precursor and CH_4 as the feedstock using a fast-heating chemical vapor deposition (CVD) method.[17] An individual thin-shelled CNT was first picked up from the substrate using a tungsten probe and then the other end of the CNT was clamped to an atomic force microscope (AFM) cantilever using electron beam induced amorphous carbon (a-C) deposition. As schematically shown

* To whom correspondence should be addressed. Phone: 86-10-62757555. Fax: 86-10-62757555. E-mail: qingchen@pku.edu.cn.
† Key Laboratory for the Physics and Chemistry of Nanodevices and Department of Electronics.
‡ College of Chemistry and Molecular Engineering.

10.1021/jp902471q CCC: $40.75
Published on Web 09/02/2009

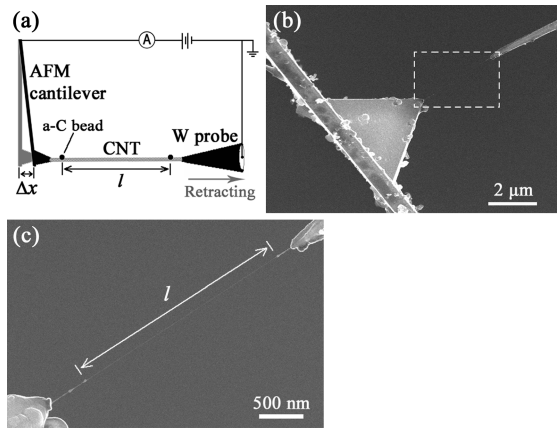

Figure 1. (a) Schematic diagram showing the setup of the measurements. (b) SEM image of a CNT under measurement. (c) Enlarged SEM images of the dashed rectangle area in (b).

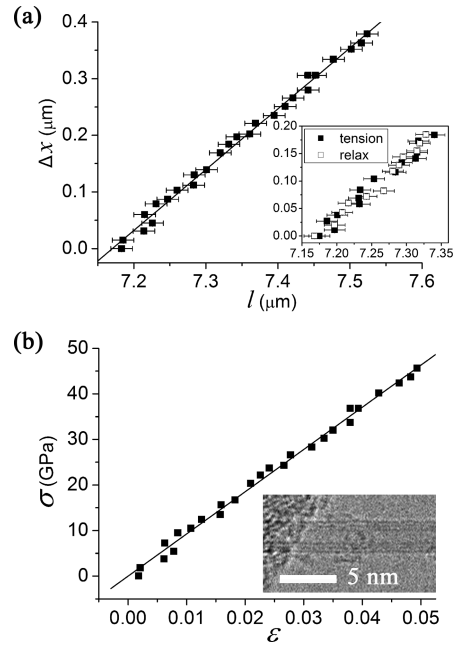

Figure 2. (a) Plot of $\Delta x-l$ data for a TWCNT. The inset shows $\Delta x-l$ data by sequential loading and relaxing the CNT at low strain. (b) The $\sigma-\varepsilon$ curve of the CNT. The inset is a TEM image of the same CNT. The solid lines in (a) and (b) are linear fitting of the experimental data.

in Figure 1a, after the tungsten probe was adjusted to be perpendicular to the AFM cantilever and aligned with the CNT, it was retracted back step-by-step along its axis to axially stretch the CNT while the clamp point of the AFM cantilever was held still. This probe movement caused the AFM cantilever to be deflected by Δx along the tube axis. For each retracting step, the length l of the CNT between two premade marks on the CNT and the displacement of the AFM probe Δx were measured in the SEM. The CNT can be loaded and relaxed repeatedly by moving the tungsten probe back and forward until it was broken. After the in situ measurement, the CNT was placed onto a transmission electron microscope (TEM) grid placed on the same SEM sample stage. SEM images were taken at different magnifications to ensure that the same CNT can be found again later. The TEM grid was then transferred into a TEM for further structure analysis. The TEM we used is a Tecnai G20 microscope. Figure 1b,c shows the SEM images of a CNT under measurement.

The spring constant of the AFM cantilever was calibrated using an in situ vibrational method.[18] A CVD synthesized MWCNT about 50 nm in diameter was first connected between the AFM cantilever to be calibrated and a tungsten probe in the same way as shown in Figure 1a, and then another tungsten probe with an alternating voltage was placed near the middle of the CNT to excite the resonance of the CNT. The first tungsten probe was retracted back step-by-step and the displacement (Δx) of the AFM probe and the resonance frequency (f) of the CNT were measured for each step. With the measured CNT lengths and diameters, the spring constant of the AFM cantilever and Young's modulus of the CNT can be obtained by fitting the measured $f-\Delta x$ data with the characteristic equation of a vibrational beam under axial tension.

Compared with previous reports,[2,4−7,16] our measurements have two improvements, which enable us to obtain more believable mechanical properties of the CNTs. First, about 2 μA current was applied to the CNTs being measured through the whole measurement process to eliminate a-C contamination induced by electron beam induced deposition (EBID) (Figure 1a).[19] The elimination of a-C contamination is achieved through increasing CNT temperature by joule heating, since the deposition rate of a-C was found to be sensitive to CNT temperature.[19] Without this anticontamination method, a layer of a-C is normally deposited on the CNT surface during measurements in SEM.[6,19] Such a layer of a-C is likely to carry load under tensile loading, and the measured breaking strength and Young's modulus may be overestimated.[6] Second, a middle section of the CNTs was marked by two a-C beads and selected for the measurement instead of the whole CNTs between the attachments (Figure 1a,c). This improvement is to remove the influence of possible slippage, which may occur at the attachments at high-strain cases and result in overestimation of breaking strain and underestimation of Young's modulus.[9] The a-C beads were deposited by focusing electron beam at the selected small area while switching off the electrical current running through the CNT.

3. Results and Discussion

Figure 2a shows a typical plot of the measured $\Delta x-l$ data for a TWCNT (the inset of Figure 2b shows the TEM image of that CNT). The length l increases linearly with Δx until the CNT is broken. The inset of Figure 2a shows the $\Delta x-l$ plots when loading and relaxing the CNT sequentially at low strain. The good linearity and overlap of the two $\Delta x-l$ plots indicate that the elongation of the CNT is elastic. A stress−strain curve of the CNT can be obtained by further analyzing the $\Delta x-l$ plot. From the linear fitting of the $\Delta x-l$ plot, we can get the initial length l_0 of the CNT at $\Delta x = 0$, then the strain ε can be calculated from $\varepsilon = (l - l_0)/l_0$. The axial tension applied to the CNTs is proportion to the displacement (Δx) of the AFM probe and can be written as $k\Delta x$, where k is the spring constant of the AFM cantilever and is well-calibrated using an in situ method.[18] The outermost shell of the TWCNT was assumed to bear load solely as in the previous reports.[2,6,16] So, the stress was calculated through $\sigma = k\Delta x/\pi Dt$, where D is the outer diameter of the CNTs and $t = 0.34$ nm is the thickness of the tube walls.[2,6,16] Figure 2b shows the $\sigma-\varepsilon$ curve of the TWCNT. The TWCNT broke at $\sigma = 4.9\%$ and $\varepsilon = 46$ GPa. Linear fitting of the $\sigma-\varepsilon$ curve gives Young's modulus of the CNT $E = 0.93$ TPa.

In total, eight individual CNTs and two CNT ropes were studied. Table 1 summarizes the results. Among the eight individual CNT samples, three CNTs slipped off from the AFM probe before breaking. As the strain of the CNT was obtained through measuring the change of the length between the two a-C beads instead of the length between the contacts with the

TABLE 1: Summary of Geometry and Mechanical Properties of All Measured CNTs

CNT type	l_0 (μm)	D (nm)	E (TPa)	ε_b (%)	σ_b (GPa)
DWCNT	3.19 ± 0.01	1.8	0.73 ± 0.07	4.4 ± 0.3	31 ± 4
DWCNT[a]	4.20 ± 0.01	2.7	1.25 ± 0.13	$>(1.5 \pm 0.2)$	$>(17 \pm 3)$
DWCNT[a]	2.63 ± 0.01	2.7	1.15 ± 0.06	$>(1.5 \pm 0.2)$	$>(17 \pm 1)$
DWCNT	2.12 ± 0.01	3.0	0.75 ± 0.04	2.8 ± 0.2	20 ± 5
TWCNT	2.73 ± 0.01	2.4	0.83 ± 0.08	1.5 ± 0.2	13 ± 1
TWCNT	3.11 ± 0.01	2.7	0.90 ± 0.08	2.3 ± 0.2	21 ± 3
TWCNT[a]	6.96 ± 0.01	2.8	1.33 ± 0.15	$>(0.9 \pm 0.1)$	$>(13 \pm 1)$
TWCNT	7.17 ± 0.01	2.8	0.93 ± 0.02	4.9 ± 0.1	46 ± 6
DWCNT+DWCNT[b]	5.48 ± 0.01	3.2	1.10 ± 0.04	$>(2.4 \pm 0.2)$	$>(28 \pm 4)$
	5.49 ± 0.01	2.4	1.71 ± 0.17	1.6 ± 0.2	23 ± 3
DWCNT+DWCNT[c]	3.84 ± 0.01	2.5	1.17 ± 0.06	3.9 ± 0.3	43 ± 5
		3.0			

[a] These CNTs slipped off from AFM probe before breaking, so that only the lower bound of the breaking strain ε_b and breaking strength σ_b were obtained. [b] The rope broke in a stepwise way. [c] The rope broke in one step.

AFM probe and tungsten probe, the slippage at the contact point does not affect the accuracy of the strain we obtained. As the displacement (Δx) of the AFM probe is much smaller than the length of the AFM cantilever, the force applied to the CNT can be written as $k\Delta x$. Because the force applied to the CNT is along its axis, the stress of the CNT section between the two a-C beads can be calculated through $\sigma = k\Delta x/\pi Dt$ even if there is a slippage at the contact point. So, the stress, strain, and Young's modulus of the three CNTs we obtained are not affected by the slippage and are accurate. However, due to the slippage, we were not able to break these three CNTs by tensile loading. Therefore, only the lower bound of the breaking strain ε_b and breaking strength σ_b was obtained for these CNTs. For the other five CNTs, ε_b ranges from 1.5 to 4.9% with an average value of 3.2% and σ_b ranges from 13 to 46 GPa with an average value of 26 GPa. The measured ε_b and σ_b vary significantly, which agrees well with the papers of Yu et al. ($\varepsilon_b \sim 3-12\%$ and $\sigma_b \sim 11-63$ GPa)[2] and Ding et al. ($\varepsilon_b \sim 1.1-6.3\%$ and $\sigma_b \sim 10-66$ GPa).[6] E of the eight individual CNTs ranges from 0.73 to 1.33 TPa with an average value of 0.98 TPa, which is in excellent agreement with previous experimental[2,6,16] and theoretical[20] reports. The variation of E is attributed to different defect levels in different CNTs. The three CNTs that slipped off from AFM probes before breaking exhibit a slightly higher Young's modulus than other CNTs. This was likely caused by the fact that those CNTs happened to have less defects.

The measured ε_b and σ_b are much lower than the theoretical results of defect-free SWCNTs predicted by various theoretical calculations,[10-15] which predicted an ε_b of about 10−30% and a σ_b of over 100 GPa. The large discrepancy between the present measured values and theoretical values is most likely caused by the defects presented in the measured CNTs, which are synthesized by CVD method. Quantum mechanics calculations predicted that the breaking strains of SWCNTs with Stone-Wales defects are only slightly decreased from those of defect-free CNTs and display no significant correlation with defect number[21] and that one- and two-atom vacancy defects could reduce ε_b by about 26% and reduce σ_b by as much as about 50%.[11] However, these defects cannot completely explain the presently measured low ε_b and σ_b. We proposed that the presently measured low ε_b and σ_b are most likely caused by larger holes. Theoretical calculations based on empirical potential predicted that the breaking strengths of SWCNTs could be reduced by more than 60% in the presence of a hole and would be much more reduced in the presence of larger holes.[11] It is reasonable that the present CVD grown CNTs containing some vacancy defects and holes. Although electron beam irradiation during in situ measurements normally causes some vacancy defects and holes in the sample, it is not the main cause for the present low ε_b and σ_b considering the special experimental setup used in the present measurements. In the present experiments, 5 KeV electron beam was used when picking up CNTs and 20 KeV electron beam was used during tensile loading the CNTs. The chamber pressure was lower than 5×10^{-4} Pa. According to the results of Yuzvinsky et al.[22] and Molhave et al.,[23] in these normal SEM observation conditions, electron beam irradiation can cause chemical damage to CNTs by producing vacancies and holes. However, such defects can be at least partly annealed by joule heating generated by the electrical current, which was used to prevent a-C contamination. Different from previous experiments, in the present experiments an electrical current of about 2 μA was applied to the CNTs through the whole measurements to prevent a-C contamination. Assuming small-diameter CNTs have the same thermal conductivity as that of SWCNTs proposed by Pop et al.[24] and connect with heat sinks with a fixed temperature 300 K at the two ends, the temperature of the CNTs due to joule heating was estimated to range from about 400 to 700 K between the two beads.[19] Adatoms were found to be able to migrate in open space between tube shells above approximately 570 K and lead to annealing of vacancy defects,[25] so vacancy defects and holes induced by electron beam irradiation can be at least partly annealed by the joule heating in the present experiments. Healing of electron beam irradiation-induced defects in SWCNTs at room temperature has also been reported previously.[26] On the other hand, the pre-existing vacancy defects and holes produced during synthesis are supposed to be unaffected by the joule heating, since no annealing of pre-existing defects has been found to take place up to at least 1000 °C during electron beam irradiation.[25]

Among all seven completed measured CNT samples, four CNTs failed in the middle section, two CNTs failed from the clamp sites of a-C, and only one failed from the mark sites of a-C beads. The breaking strains and strengths of the three CNTs, which failed from the clamp or mark sites, are not markedly lower than those of the CNTs failed in the middle section. Therefore, possible stress concentration or defects induced by a-C deposition at the clamp or mark sites are not the cause of the present measured low breaking strain and strength.

Individual DWCNTs and TWCNTs mostly broke in a "sword-in-sheath"[2] way with a sudden one-step decrease of Δx to nearly zero. Here, we observed that CNT ropes exhibited one-step or stepwise breaks depending on the relative breaking strains of the two CNTs. If the two CNTs in a rope have similar breaking strains, the break of one CNT will cause the subsequent break of the other one and the rope would break in one step and have a similar $\Delta x-l$ plot to those of individual CNTs. If the breaking

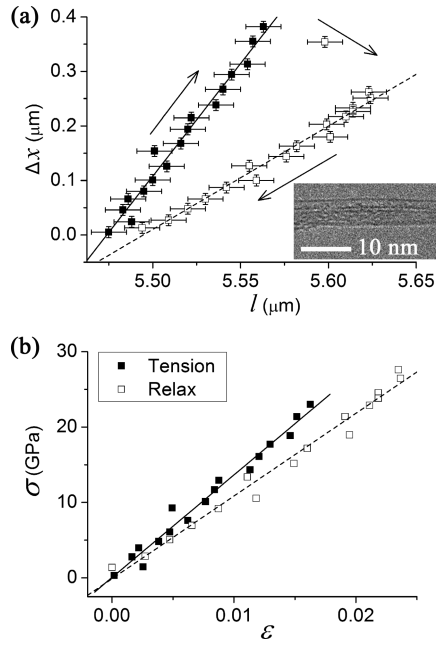

Figure 3. (a) Plot of $\Delta x-l$ data of a CNT rope broken stepwise. The arrows indicate the direction of the measurement. The solid points were measured during loading, while hollow points were measured during relaxing. The inset shows a TEM image of the same rope consisting of two DWCNTs. (b) The $\sigma-\varepsilon$ curve of the CNT rope under loading (solid points) and relaxing (hollow points). The lines in (a) and (b) are linear fitting of the experimental data.

strains of the two CNTs differ obviously from each other, the CNT rope will break stepwise.

Figure 3a shows the $\Delta x-l$ plots of a CNT rope consisting of two DWCNTs with D of 2.4 nm and 3.2 nm (shown in the inset of Figure 3a). The arrows indicate the direction of the measurement. The rope was first axially stretched with the tungsten probe being moved backward. We observed that l increases linearly first with Δx; then, a sudden increase of l happened together with a sudden decrease of Δx. We then relaxed the CNT by moving the tungsten probe forward and observed that l decreases linearly with the decrease of Δx to the initial length but with a smaller slope compared with that during loading. The sudden increase of l and decrease of Δx indicate that one of the two CNTs was broken at that moment. At the beginning, the two CNTs carried load together showing larger rigidity during loading, while during relaxation, only one CNT carried load showing smaller rigidity.

Assuming that the outer shells of the two CNTs in the ropes carried load together, $\sigma-\varepsilon$ curves of the CNT ropes can be calculated from their $\Delta x-l$ plots and Young's modulus of the CNT ropes was obtained from linear fitting of the $\sigma-\varepsilon$ curves. For the rope shown in Figure 3a, which broke in a stepwise way, assuming that the thinner CNT broke first, the $\sigma-\varepsilon$ curves under both loading and relaxing were calculated from the $\Delta x-l$ plots and shown in Figure 3b. From the $\sigma-\varepsilon$ curve under relaxation, $E = 1.10$ TPa, $\varepsilon_b > 2.4\%$, and $\sigma_b > 28$ GPa were obtained for the thicker CNT. From the $\sigma-\varepsilon$ curve under loading, $\varepsilon_b = 1.6\%$ and $\sigma_b = 23$ GPa were obtained for the thinner CNT, and $E = 1.36$ TPa were obtained for the whole rope. The large discrepancy between the breaking strains of the two CNTs caused the stepwise break of the rope. Assuming that the two CNTs in the rope carry load independently, E of the thinner CNT was calculated to be 1.71 TPa, which is much larger than that of other CNTs and was possibly overestimated by the twist of the two CNTs in the rope. When CNT ropes are axially stretched, twist of CNTs was predicted to cause the collapse of tube cross section,[27] which will increase the van der Waals interaction and thus load transfer between shells. So, Young's modulus was overestimated when assuming that only the outer shells carry load. Stepwise breakage reduces the strength of the CNT ropes due to the earlier break of part of the CNTs in the ropes. So, it is important for the CNTs in a rope to have similar breaking strains in the applications of CNT rope, such as reinforcements in composites.

4. Conclusion

In conclusion, breaking strain and strength and Young's modulus of individual DWCNTs, TWCNTs, and CNT ropes consisting of only two DWCNTs were measured by tensile loading. The measured breaking strain and strength are much lower than that of defect-free SWCNTs predicted by theory. The low breaking strain and strength are attributed to the defects presented in the CVD grown CNTs. CNT ropes exhibited stepwise break when the breaking strains of the CNTs differ much from each other. Such a stepwise break can reduce the strength of the CNT ropes and should be prevented in the applications of CNT ropes.

Acknowledgment. This work was supported by the NSF China (60771005 and 60728102), the NSF Beijing, China (4092023) and the MOST (2009AA03Z315 and 2006CB932401).

References and Notes

(1) Coleman, J. N.; Khan, U.; Gun'ko, Y. K. *Adv. Mater.* **2006**, *18*, 689.
(2) Yu, M. F.; Lourie, O.; Dyer, M. J.; Moloni, K.; Kelly, T. F.; Ruoff, R. S. *Science* **2000**, *287*, 637.
(3) Huang, J. Y.; Chen, S.; Wang, Z. Q.; Kempa, K.; Wang, Y. M.; Jo, S. H.; Chen, G.; Dresselhaus, M. S.; Ren, Z. F. *Nature* **2006**, *439*, 281.
(4) Demczyk, B. G.; Wang, Y. M.; Cumings, J.; Hetman, M.; Han, W.; Zettl, A.; Ritchie, R. O. *Mater. Sci. Eng.* **2002**, *A334*, 173.
(5) Barber, A. H.; Andrews, R.; Schadler, L. S.; Wagner, H. D. *Appl. Phys. Lett.* **2005**, *87*, 203106.
(6) Ding, W.; Calabri, L.; Kohlhaas, K. M.; Chen, X.; Dikin, D. A.; Ruoff, R. S. *Exp. Mech.* **2007**, *47*, 25.
(7) Yu, M. F.; Files, B. S.; Arepalli, S.; Ruoff, R. S. *Phys. Rev. Lett.* **2000**, *84*, 5552.
(8) Walters, D. A.; Ericson, L. M.; Casavant, M. J.; Liu, J.; Colbert, D. T.; Smith, K. A.; Smalley, R. E. *Appl. Phys. Lett.* **1999**, *74*, 3803.
(9) Belytschko, T.; Xiao, S. P.; Schatz, G. C.; Ruoff, R. S. *Phys. Rev. B* **2002**, *65*, 235430.
(10) Ogata, S.; Shibutani, Y. *Phys. Rev. B* **2003**, *68*, 165409.
(11) Mielke, S. L.; Troya, D.; Zhang, S.; Li, J.; Xiao, S.; Car, R.; Ruoff, R. S.; Schatz, G. C.; Belytschko, T. *Chem. Phys. Lett.* **2004**, *390*, 413.
(12) Zhao, Q. Z.; Nardelli, B. M.; Bernholc, J. *Phys. Rev. B* **2002**, *65*, 144105.
(13) Samsonidze, G. G.; Samsonidze, G. G.; Yakobson, B. I. *Phys. Rev. Lett.* **2002**, *88*, 065501.
(14) Wei, C.; Cho, K.; Srivastava, D. *Phys. Rev. B* **2003**, *67*, 115407.
(15) Dumitrica, T.; Yakobson, B. I. *Appl. Phys. Lett.* **2004**, *84*, 2775.
(16) Peng, B.; Locascio, M.; Zapol, P.; Li, S.; Mielke, S. L.; Schatz, G. C.; Espinosa, H. D. *Nat. Nanotechnol.* **2008**, *3*, 626.
(17) Zhou, W. W.; Han, Z. Y.; Wang, J. Y.; Zhang, Y.; Jin, Z.; Sun, X.; Zhang, Y. W.; Yan, C. H.; Li, Y. *Nano Lett.* **2006**, *6*, 2987.
(18) Wei, X. L.; Chen, Q.; Xu, S. Y.; Peng, L.-M.; Zuo, J. M. *Adv. Funct. Mater.* **2009**, *19*, 1753.
(19) Wei, X. L.; Liu, Y.; Chen, Q.; Peng, L.-M. *Nanotechnology* **2008**, *19*, 355304.
(20) Lu, J. P. *Phys. Rev. Lett.* **1997**, *79*, 1297.
(21) Troya, D.; Mielke, S. L.; Schatz, G. C. *Chem. Phys. Lett.* **2003**, *382*, 133.
(22) Yuzvinsky, T. D.; Fennimore, A. M.; Mickelson, W.; Esquivias, C.; Zettl, A. *Appl. Phys. Lett.* **2005**, *86*, 053109.
(23) Molhave, K.; Gudnason, S. B.; Pedersen, A. T.; Clausen, C. H.; Horsewell, A.; Boggild, P. *Ultramicroscopy* **2007**, *108*, 52.
(24) Pop, E.; Mann, D.; Wang, Q.; Goodson, K.; Dai, H. J. *Nano Lett.* **2006**, *6*, 96.
(25) Banhart, F. *Rep. Prog. Phys.* **1999**, *62*, 1181.
(26) Suzuki, S.; Kobayashi, Y. *J. Phys. Chem. C* **2007**, *111*, 4524.
(27) Qian, D.; Liu, W. K.; Ruoff, R. S. *Compos. Sci. Technol.* **2003**, *63*, 1561.

JP902471Q